Frontiers in Bioscience Landmark

Front. Biosci. (Landmark Ed) **2026**; 31(8): 53201
https://doi.org/10.31083/FBL53201

Original Research

Calcium-Sensing Receptor Activation Disrupts Phosphatidylserine Asymmetry and Promotes Calcium Oxalate Crystal–Induced Epithelial Injury in Renal Tubular Epithelial Cells

Hanlin Liu[1,2,†], Yangjie Xiao[1,2,†], Yuqiang Fu[1,2], Siyu Chen[1,2], Wei Shi[1,2,*], Xiaoran Li[1,2,*]

[1]Department of Urology, The Second Hospital & Clinical Medical School, Lanzhou University, 730000 Lanzhou, Gansu, China
[2]Institute of Urology, Gansu Province Clinical Research Center for Urinary System Diseases, The Second Hospital of Lanzhou University, 730030 Lanzhou, Gansu, China
*Correspondence: shiweijust@126.com (Wei Shi); lixiaoran05@163.com (Xiaoran Li)
[†]These authors contributed equally.
Academic Editor: Guoping Zheng
Submitted: 22 April 2026 Revised: 26 May 2026 Accepted: 4 June 2026 Published: 17 August 2026

Abstract

Background: Calcium oxalate (CaOx) crystal retention on the renal tubular epithelium is a key step in urolithiasis. Phosphatidylserine (PS) exposure may facilitate crystal–cell adhesion, but the upstream signaling mechanisms and the relative contributions of impaired inward PS flipping versus outward PS redistribution remain unclear. **Materials and Methods:** Global proteomic profiling using 2-dimensional electrophoresis and matrix-assisted laser desorption/ionization time-of-flight/time-of-flight mass spectrometry (2-DE/MALDI-TOF/TOF) in an immortalized human proximal tubular epithelial cell line (HK-2) cells exposed to calcium oxalate monohydrate (COM) identified upregulation of the calcium-sensing receptor (CaSR). HK-2 cells were treated with COM with or without the CaSR antagonist NPS2390 or the CaSR agonist gadolinium chloride ($GdCl_3$). Bidirectional PS transport was assessed using an N-(7-nitrobenz-2-oxa-1,3-diazol-4-yl) (NBD)-labeled phosphatidylserine (NBD-PS) fluorescence-quenching assay, and surface PS exposure was measured by annexin V binding. Aminophospholipid translocase (APLT) expression, APLT-dependent inward PS transport, crystal adhesion, oxidative stress, and apoptosis-related signaling were evaluated. **Results:** COM increased CaSR expression, enhanced surface PS exposure, and promoted crystal adhesion with concurrent oxidative stress and apoptosis-related signaling. COM induced a CaSR-sensitive defect in APLT-dependent inward PS flipping: NPS2390 partially restored inward PS transport and APLT expression, whereas $GdCl_3$ exacerbated these changes. In contrast, COM-enhanced outward PS redistribution and externalization was largely unaffected by CaSR modulation, indicating relative CaSR insensitivity of the outward process. Consistently, CaSR activation aggravated, while CaSR inhibition attenuated, crystal adhesion and injury-related readouts. **Conclusions:** COM was associated with enhanced crystal–cell adhesion, CaSR activation, and a CaSR-sensitive impairment of APLT-dependent inward PS flipping, whereas enhanced outward PS redistribution appeared largely CaSR-insensitive. Pharmacologic inhibition of CaSR attenuated epithelial injury and crystal retention-related readouts, suggesting that CaSR may represent a potential therapeutic target.

Keywords: urinary calculi; calcium oxalate; calcium-sensing receptor; phosphatidylserines; reactive oxygen species; apoptosis

1. Introduction

Urolithiasis mainly involves calcium oxalate (CaOx) crystal formation and is often related to metabolic disorders such as hypocitraturia, hyperoxaluria and hypercalciuria [1]. Beyond crystal formation, stone pathogenesis critically depends on crystal retention within the kidney, which is largely driven by interactions between CaOx crystals and renal tubular epithelial cells [2].

Under appropriate conditions, calcium oxalate monohydrate (COM) crystals can adhere directly to viable tubular epithelial cells [3,4]. Rather than being explained solely by nonspecific physical trapping, COM retention is influenced by crystal–cell interactions at the apical membrane, including surface binding sites and other membrane-associated factors [5]. Accumulating evidence suggests that COM crystal exposure is associated with phosphatidylserine (PS) appearance on the outer leaflet of renal epithelial membranes, providing an anionic surface that may favor crystal attachment and thereby facilitate COM crystal retention [6,7].

PS is normally confined to the inner leaflet of the plasma membrane, and its externalization provides a negatively charged surface that can facilitate calcium oxalate crystal attachment [8]. Membrane lipid asymmetry is maintained by aminophospholipid translocase (APLT)-dependent inward flipping of PS, whereas surface PS exposure may also reflect outward lipid redistribution under injury conditions [9].

Oxidative stress (OS) and intracellular reactive oxygen species (ROS) have been implicated in calcium oxalate–induced epithelial injury and can impair APLT ac-

tivity, thereby promoting PS externalization in renal tubular epithelial cells [10]. Accordingly, dissecting whether COM-induced surface PS accumulation reflects impaired inward flipping versus additional outward redistribution provides a mechanistic framework for interpreting crystal–cell interactions in our model [9,11].

However, during kidney-stone formation, multiple molecules and signaling pathways participate in the complex interactions between CaOx crystals and renal tubular epithelial cells, and the upstream regulators linking crystal exposure to epithelial injury and crystal retention remain incompletely defined. Given the multifactorial nature of these responses, an unbiased screening strategy may help identify additional candidate regulators beyond previously studied single targets.

In this study, we profiled global protein changes in HK-2 cells exposed to a high-COM environment using 2-DE coupled with MALDI-TOF/TOF, and prioritized candidates with plausible membrane-signaling relevance and pharmacologic tractability. Among the identified candidates, we focused on the calcium-sensing receptor (CaSR), because CaOx has been reported to induce renal injury through CaSR signaling and CaSR activation is implicated in crystal retention-related responses [12]. Moreover, CaSR provides a receptor-level, pharmacologically tractable entry point for mechanistic testing.

Because PS exposure is a canonical "eat-me" signal in apoptosis and can also occur in regulated non-apoptotic cell-death contexts, PS externalization provides a mechanistically relevant readout of epithelial injury in crystal/oxalate stress models [13,14]. In parallel, CaOx/oxalate exposure engages oxidative-stress pathways (including NADPH oxidase–related responses), and antioxidant defenses can mitigate oxalate/ CaOx-induced epithelial injury [15,16,17,18]. Accordingly, we pharmacologically modulated CaSR using NPS2390 or $GdCl_3$ and assessed its effects on PS exposure, crystal adhesion, and oxidative/apoptosis-related readouts.

2. Materials and Methods

2.1 Crystal Preparation

COM crystals were prepared as previously described [19]. Equal volumes of sodium oxalate (10 mM) and $CaCl_2$ (10 mM) were mixed at approximately 26 °C, and the resulting crystals were incubated at 4 °C for approximately 3 days. The crystals were washed with deionized water and dried at 62 °C. Fourier-transform infrared spectroscopy (FTIR; Thermo Fisher Scientific, Waltham, MA, USA) was used to confirm that the crystals were COM. A COM stock suspension was prepared in sterile phosphate-buffered saline (PBS) at 5 mg/mL. For treatment, COM crystals were evenly added to the cell monolayer at a surface dose of 67 μg/cm^2, and PBS was added to keep the final volume consistent among groups.

2.2 Cell Culture

HK-2 cells, a human proximal tubular epithelial cell line, were obtained from the American Type Culture Collection (ATCC, Manassas, VA, USA) and cultured in Dulbecco's modified Eagle's medium (DMEM; Gibco, Thermo Fisher Scientific, Waltham, MA, USA) supplemented with 10% fetal bovine serum (FBS; Gibco, Catalog No. A5256901) and 1% penicillin–streptomycin (Gibco, Catalog No. 15140-122) at 37 °C in a humidified incubator (model CLM-240B-8-CN, Esco, Singapore) with 5% CO_2. The cell line was verified by short tandem repeat (STR) profiling and tested negative for mycoplasma contamination before use in the experiments.

2.3 Protein Extraction, Two-Dimensional Gel Electrophoresis (2-DE) and Staining

HK-2 cells were cultured with or without COM crystals at 67 μg/cm^2 for 24 h. Cells were then collected in PBS containing 0.5 M EDTA and incubated at 4 °C for 30 min to remove attached crystals. After washing to remove residual EDTA, cells were resuspended in lysis buffer and incubated at 4 °C for 40 min. The lysates were centrifuged to remove insoluble debris.

For 2-DE analysis, proteins were first separated by isoelectric focusing according to their isoelectric points and then by SDS-PAGE according to molecular weight. Protein samples were mixed with 2D lysis buffer containing protease inhibitors and concentrated using 10-kDa ultrafiltration tubes by centrifugation at 13,000 ×g for 20 min at room temperature. This concentration step was repeated twice, and protein concentration was determined using the Bradford method.

A total of 300 μg protein was loaded onto nonlinear pH 3–10 gradient strips. Isoelectric focusing was performed sequentially at 30 V for 12 h, 500 V for 1 h, 1000 V for 1 h, 8000 V for 8 h, and 500 V for 4 h. SDS-PAGE was then performed using 12.5% gels at 15 mA for 30 min and then 30 mA until the bromophenol blue front reached approximately 0.5 cm from the gel edge. Gels were stained using a rapid silver-staining protocol and then scanned for image analysis.

2.4 Image Analysis and Protein Identification by MALDI-TOF/TOF

Differential protein spots were excised from silver-stained gels and subjected to in-gel tryptic digestion. Gel pieces were destained, washed with 100 mM NH_4HCO_3, and incubated at room temperature for 15 min. Sequencing-grade trypsin solution (Promega, Madison, WI, USA) was then added, and digestion was performed overnight at 37 °C for approximately 20 h. Peptides were extracted with 60% acetonitrile/ 0.1% trifluoroacetic acid under ultrasonication, lyophilized, and desalted using ZipTips (Millipore, Billerica, MA, USA) when necessary.

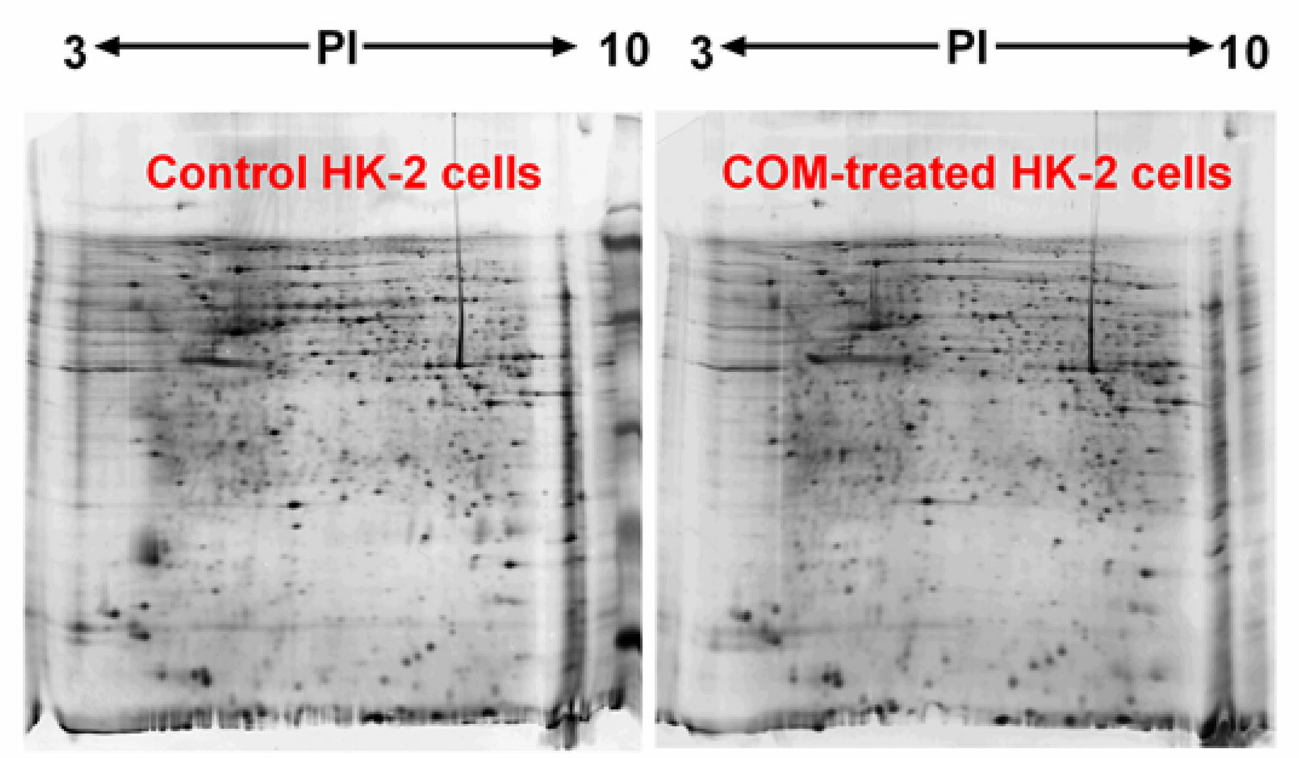

Fig. 1. 2-DE maps of proteins from COM-treated human renal epithelial cells and control human renal epithelial cells. Confluent human renal epithelial cells were exposed to COM crystals (67 μg/cm^2) for 24 h. Untreated human renal epithelial cells served as controls. Twenty-four hours later, cell lysates were prepared for two-dimensional gel electrophoresis, and proteins were visualized by silver staining.

For mass spectrometry analysis, dried peptide samples were dissolved in 20% acetonitrile. One microlitre of each sample was spotted onto a 384 Opti-TOF stainless-steel target plate (AB SCIEX, Framingham, MA, USA) and air-dried, followed by the addition of 0.5 μL saturated CHCA matrix solution prepared in 50% acetonitrile in 0.1% trifluoroacetic acid. Samples were analyzed using a 5800 MALDI-TOF/TOF mass spectrometer (AB SCIEX, Framingham, MA, USA) equipped with a 355-nm Nd: YAG laser. Data were acquired in positive-ion reflector and automatic acquisition modes over an MS range of 800–4000 Da. Parent ions with signal-to-noise ratios greater than 50 were selected for MS/MS analysis, with up to eight parent ions analyzed per sample spot. Protein identification was performed using MASCOT 2.2 software (version 2.2; Matrix Science Ltd., London, UK) against the NCBI Protein database (https://www.ncbi.nlm.nih.gov/protein/).

2.5 Annexin V Binding Analysis

Cell-surface PS exposure was assessed using FITC-labelled Annexin V staining. HK-2 cells were grown to approximately 80% confluence and treated with COM crystals at 67 μg/cm^2. for 24 h. For CaSR modulation, cells were pretreated with NPS2390 at 10 μM for 1 h or with $GdCl_3$ at 300 μM for 30 min before COM exposure. After treatment, cells were stained with Annexin V-FITC in binding buffer and incubated for 15 min in the dark.

Annexin V fluorescence was measured by flow cytometry at an excitation wavelength of 488 nm and an emission wavelength of 530 nm. The Annexin V-FITC-positive threshold was set using a calcium-depleted negative control, in which 2.5 mM EDTA replaced 2.5 mM $CaCl_2$ during Annexin V-FITC staining. For each sample, 5000 events were acquired and analyzed using CellQuest Pro software. The percentage of Annexin V-positive cells was used as an index of cell-surface PS exposure. Because viability dyes such as PI or 7-AAD were not included, this assay was not intended to define cell-death stages.

2.6 Determination of the Levels of Malondialdehyde (MDA), Superoxide Dismutase (SOD) and Lactate Dehydrogenase (LDH)

Malondialdehyde (MDA), superoxide dismutase (SOD), and lactate dehydrogenase (LDH) levels were measured using commercial assay kits according to the manufacturers' instructions.

2.7 Labelling of HK-2 Cells With NBD-Labelled PS

Bidirectional PS transport was assessed using the fluorescent PS analogue nitrobenzoxadiazole-labeling phos-

Table 1. Summary of significantly altered proteins in HK-2 cells in response to high COM exposure.

Spot no.	Gene symbol	Protein	NCBI entry	Protein MW	Protein PI	No. of identified peptides	Protein Score	Protein Score C. I. %	Intensity Matched	Total Ion Score	Degree of change (fold)
1980	*HADH2*	hydroxyacyl-Coenzyme A dehydrogenase, type II, isoform CRA_b	gi|119613564	26,195.7	6.73	5	248	100	10.737	226	3.01400
1398	*ANXA2*	annexin A2 isoform 2	gi|50845386	38,807.9	7.57	20	352	100	19.852	246	2.19216
1406	*CASR*	calcium-sensing receptor	gi|37577159	122,493.2	6.57	10	200	100	12.257	176	1.73504
607	*LMNA*	lamin isoform C	gi|5031875	65,152.6	6.4	23	99	99.995	5.5	20	1.63278
1300	*ANXA2*	annexin A2, isoform CRA_a	gi|119597988	40,670.8	8.53	22	1000	100	55.577	873	1.59897
1916	*PRDX1*	peroxiredoxin-1	gi|32455266	22,324.4	8.27	15	313	100	15.829	199	–1.58798
1586	*PSMA1*	proteasome subunit alpha type-1 isoform 3	gi|221316716	14,728.6	8.69	8	220	100	10.177	168	1.57837
1744	ACTG1	Actin, cytoplasmic 2	gi|54036678	42,107.9	5.31	10	321	100	19.782	278	1.54370
1331	ACTG1	Actin, cytoplasmic 2	gi|316659409	42,107.9	5.31	10	584	100	25.528	543	1.51170
1717	*ETFB*	electron transfer flavoprotein subunit beta isoform 2	gi|62420877	37,753.1	6.78	10	314	100	13.045	273	1.51036

phatidylserine (NBD-PS) [20,21]. NBD-PS dissolved in chloroform was dried under nitrogen and reconstituted in anhydrous ethanol at 6 nmol per 2×10^7 cells. Cells were divided into two labelling groups to assess inward and outward PS movement separately.

For inward transport analysis, NBD-PS was incorporated into the outer leaflet of the plasma membrane. Cells were cooled to 2 °C to reduce inward PS movement, incubated with NBD-PS in modified PBS (mPBS) for 15 min on ice, and then washed with ice-cold mPBS to remove unincorporated NBD-PS.

For outward transport analysis, NBD-PS was first incorporated into the inner leaflet. Cells were incubated with NBD-PS in mPBS containing 5 mM diisopropyl fluorophosphate at 37 °C for 1 h to prevent NBD-PS degradation. After NBD-PS accumulation in the inner membrane, cells were washed three times with mPBS containing 1% BSA to remove residual NBD-PS from the outer plasma membrane.

2.8 Fluorescence Quenching and PS Translocation Analysis

To assess inward PS movement, outer leaflet-labelled cells were treated with COM crystals in the presence or absence of $GdCl_3$ or NPS2390. For $GdCl_3$ treatment, cells were pretreated with $GdCl_3$ at 300 µM for 30 min before COM exposure. For NPS2390 treatment, cells were pretreated with NPS2390 at 10 µM for 60 min before COM exposure.

At each time point, aliquots of cell suspension were collected and fluorescence was measured using a fluorescence spectrophotometer with excitation at 470 nm and emission at 530 nm. Total fluorescence (FT) was recorded during the first 50 s. Fresh sodium dithionite was then added to a final concentration of 25 mM in 1 M Tris buffer, pH 10, to quench NBD fluorescence on the cell surface. The fluorescence after dithionite treatment (FD) was recorded over 240 s. Triton X-100 was subsequently added to permeabilize the membrane and allow quenching of internal NBD fluorescence, and the residual fluorescence (F0) was recorded during the first 50 s. The percentage of NBD-PS in the inner membrane was calculated as follows: inner percentage = $100 \times [(FD - F0)/(FT - F0)]$.

To assess outward PS movement, inner leaflet-labelled cells were incubated in mPBS containing 1% BSA. Aliquots were collected at 0, 2, 6, 8, 12, 18, and 24 h for fluorescence measurement, and the percentage of NBD-PS exposed on the outer membrane was calculated as follows: outer percentage = $100 \times [(FT - FD)/(FT - F0)]$.

2.9 Western Blot Analysis

Total protein was extracted according to standard procedures, and protein concentration was determined using the Bradford method. Equal amounts of protein, 20 µg per lane, were separated by 10% SDS-PAGE and transferred onto nitrocellulose membranes at 100 V for 1 h using a water-cooled transfer system.

Membranes were blocked with 5% skim milk in TBS-T for 1 h at 37 °C and incubated with primary antibodies overnight at 4 °C. Details of the primary antibodies, including the product number, vendor, and dilution rate, are provided in **Supplementary Table 1**. After three washes with TBS-T, membranes were incubated with alkaline phosphatase-conjugated secondary antibodies diluted 1:1000 in TBS-T for 1 h at 20 °C. Protein bands were visualized using Western Blue stabilized alkaline phosphatase substrate. Band densities were quantified using a Bio-Rad ChemiDoc EQ densitometer and Quantity One software.

2.10 Crystal Adhesion Assay

Crystal adhesion was assessed using a previously described method [22]. After 24 h of culture, HK-2 cells were divided into four groups: Control, COM, COM+$GdCl_3$, and COM+NPS2390. Control cells were cultured in DMEM alone. Cells in the COM group were treated with COM crystals at 67 µg/cm^2. Cells in the COM+$GdCl_3$ group were pretreated with $GdCl_3$ at 300 µM for 30 min before COM exposure. Cells in the COM+NPS2390 group were pretreated with NPS2390 at 10 µM for 1 h before COM exposure.

After exposure to COM crystals for 6, 12, 24, or 48 h, unbound crystals were removed and collected. Crystals were counted under a phase-contrast microscope in five randomly selected high-power fields. The number of unbound crystals was used to infer crystal adhesion/retention on the cell monolayer. Experiments were performed in triplicate.

2.11 Statistical Analyses

Quantitative data are presented as mean ± standard error of the mean (SEM). Statistical analyses were performed using SPSS (version 13.0). For comparisons among multiple groups, one-way analysis of variance (ANOVA) was applied, followed by an appropriate post hoc multiple-comparison test. For comparisons between two groups, a two-tailed Student's *t*-test was used. A two-sided $p < 0.05$ was considered statistically significant.

3. Results

3.1 Proteomic Analysis

By spot matching, approximately 900 protein spots were detected on each 2-DE gel (Fig. 1). Using quantitative spot-intensity analysis and MALDI-TOF/TOF identification, 10 differential protein spots showing changes of >1.5-fold were successfully identified and corresponded to 8 unique proteins (with some proteins appearing as multiple spots), including seven upregulated and one downregulated protein. Detailed identification information, including peptide numbers, protein scores, and fold changes, is summarized in Table 1.

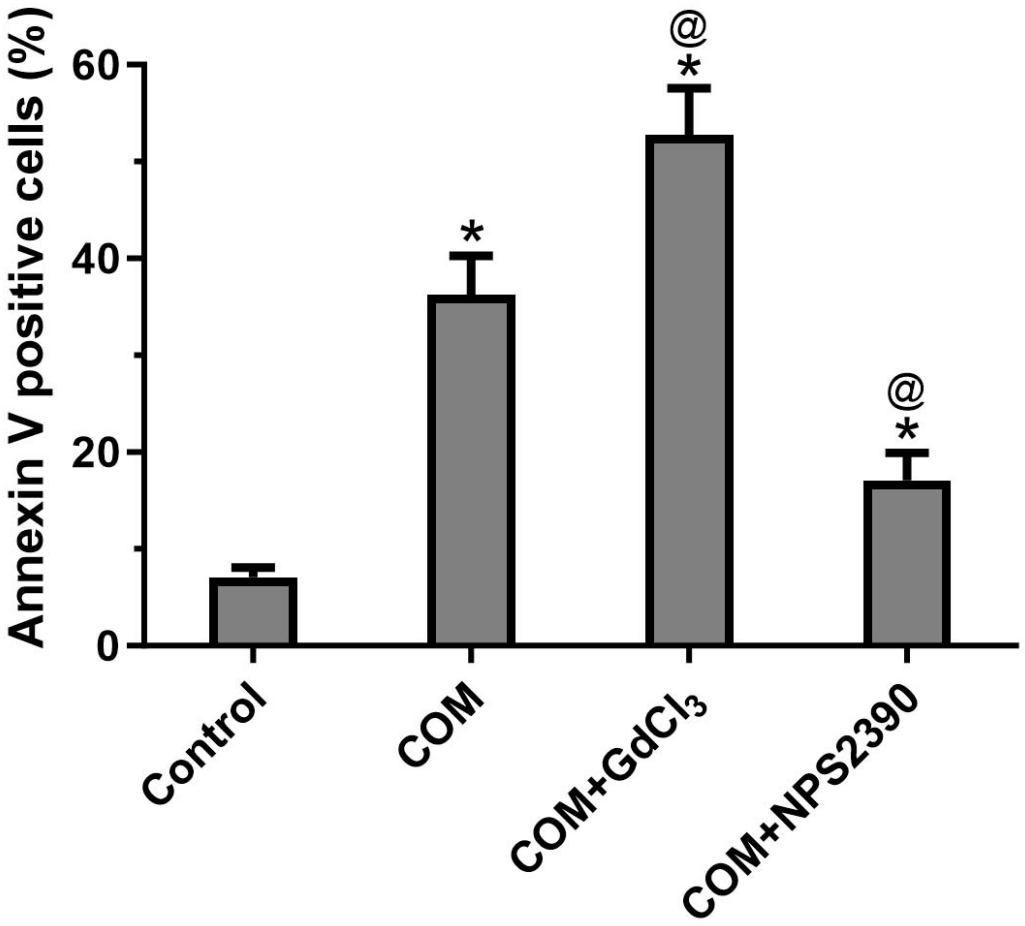

Fig. 2. COM-induced PS exposure in human renal epithelial cells. Surface PS exposure was assessed by Annexin V-FITC staining and flow cytometry. Annexin V-positive cells were quantified by flow cytometry and expressed as the percentage of PS-externalized cells. (1) In the Control group, human renal epithelial cells were cultured in medium for 24 h at 37 °C. (2) In the COM group, human renal epithelial cells were treated with COM crystals (67 μg/cm^2) for 24 h at 37 °C. (3) In the COM+$GdCl_3$ group, human renal epithelial cells were pretreated with $GdCl_3$ (300 μM) for 30 min and then treated with COM crystals (67 μg/cm^2) for 24 h at 37 °C. (4) In the COM+NPS2390 group, human renal epithelial cells were pretreated with NPS2390 (10 μM) for 1 h and then treated with COM crystals (67 μg/cm^2) for 24 h at 37 °C. Data are presented as mean ± SEM from three independent biological replicates. *$p < 0.05$ versus Control; $^{@}p < 0.05$ versus COM.

3.2 PS Exposure

Annexin V-FITC binds to cell-surface PS and was therefore used to assess PS exposure. Human renal epithelial cells were treated with COM crystals (67 μg/cm^2) for 24 h, and PS exposure was assessed using flow cytometry. The number of Annexin V-FITC-positive cells was lower in the control group than in the COM group ($p < 0.05$). These results indicate that COM treatment increased cell-surface PS exposure in human renal epithelial cells.

PS exposure was higher in the COM+$GdCl_3$ group but lower in the COM+NPS2390 group than in the COM group ($p < 0.05$), suggesting that pharmacologic CaSR modulation was associated with changes in surface PS exposure under COM-treated conditions (Fig. 2).

3.3 OS Levels

LDH and MDA levels were significantly higher in the COM group than in the control group, whereas SOD activity was significantly lower ($p < 0.05$). Compared with COM alone, $GdCl_3$ further increased LDH and MDA levels and decreased SOD activity ($p < 0.05$). In contrast, NPS2390 reduced LDH and MDA levels and restored SOD activity compared with COM alone ($p < 0.05$) (Fig. 3).

3.4 NBD-PS Inward Movement

Fluorescent NBD-PS was incorporated into the outer membrane leaflet to assess whether COM crystals affected inward PS transport, and PS internalization was monitored over time (Fig. 4A). Approximately 90% of NBD-PS was internalized by human renal epithelial cells within 24 h (Fig. 4B). However, under COM treatment (67 μg/cm^2), the per-

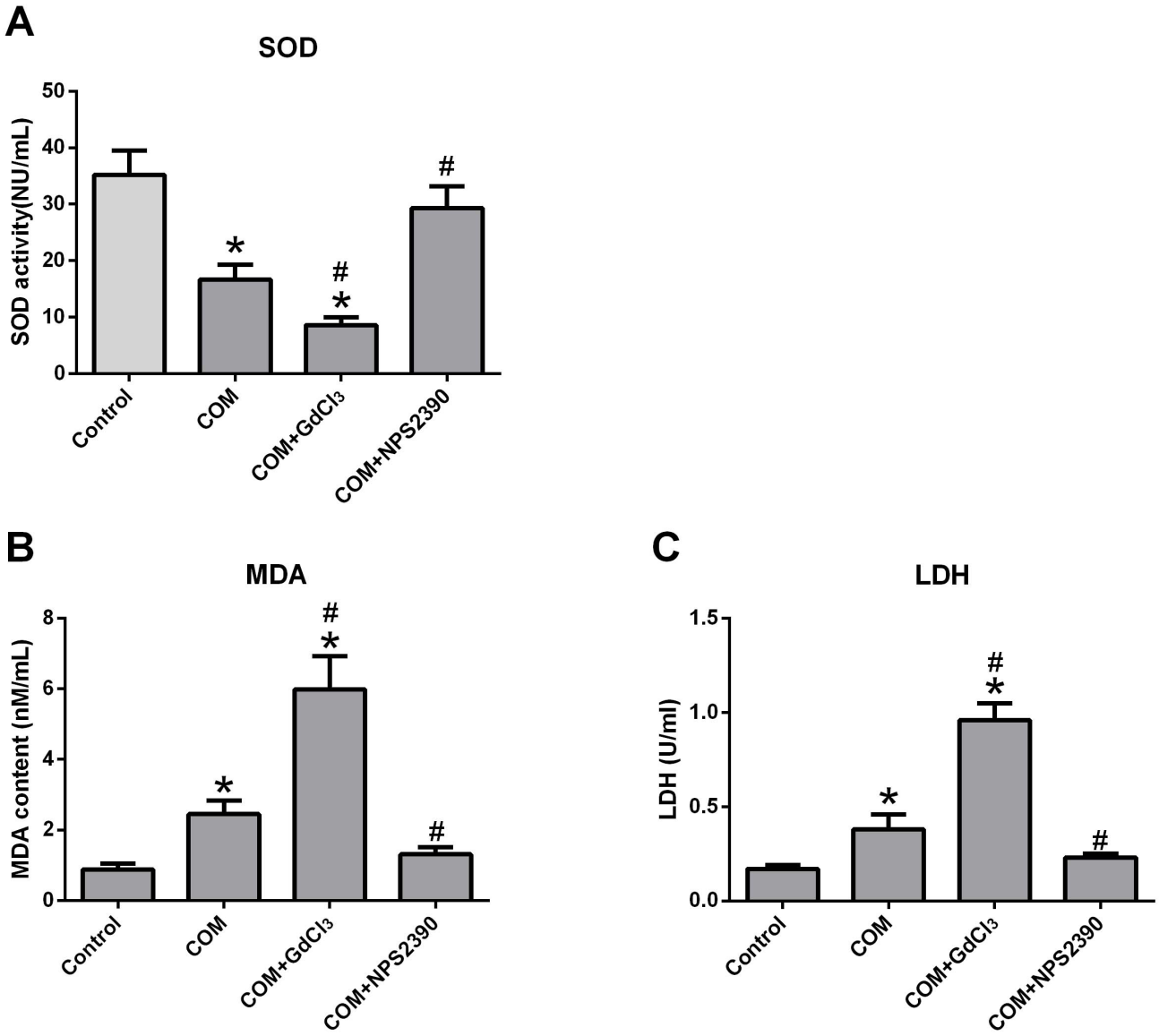

Fig. 3. Effects of COM and CaSR modulation on oxidative-stress-related readouts in HK-2 cells. Cells were treated with COM crystals (67 μg/cm^2) for 24 h in the presence or absence of $GdCl_3$ (300 μM, 30 min pretreatment) or NPS2390 (10 μM, 1 h pretreatment). (A) SOD activity in cells. (B) MDA content in cells. (C) LDH content in the culture medium. Data are presented as mean ± SEM from three independent biological replicates. *$p < 0.05$ versus Control; $^{\#}p < 0.05$ versus COM.

centage of internalized NBD-PS decreased to 48% (Fig. 4B) ($p < 0.05$). The inward transport rate of PS increased after the addition of the CaSR inhibitor NPS2390 to COM-treated cells ($p < 0.05$). In the COM+NPS2390 group, approximately 71% of NBD-PS was internalized, which was very similar to the percentage observed in the control group. In contrast, the addition of the CaSR activator $GdCl_3$ to COM-treated cells inhibited the inward transport of PS ($p < 0.05$) (Fig. 4B).

We also preincubated cells with the APLT inhibitor N-ethylmaleimide (NEM) (5 mM, 15 min) and tested the inward movement of NBD-PS. After NEM was added, the intrinsic kinetics became similar regardless of the presence or absence of other agents and were lower than the control values ($p < 0.05$, Fig. 4B). These results suggest that inward NBD-PS movement in human renal epithelial cells is largely APLT-dependent and that pharmacologic CaSR modulation is associated with altered APLT-dependent inward PS transport under COM-treated conditions.

3.5 NBD-PS Outward Movement

To assess outward PS movement, NBD-PS was incorporated into the inner membrane leaflet, and its redistribution to the outer leaflet was monitored over time. This assay was used to determine whether COM altered outward PS transport and whether this process was affected by CaSR modulation. The incubation medium contained BSA (1% w/v), which rapidly extracts cell-surface NBD-PS

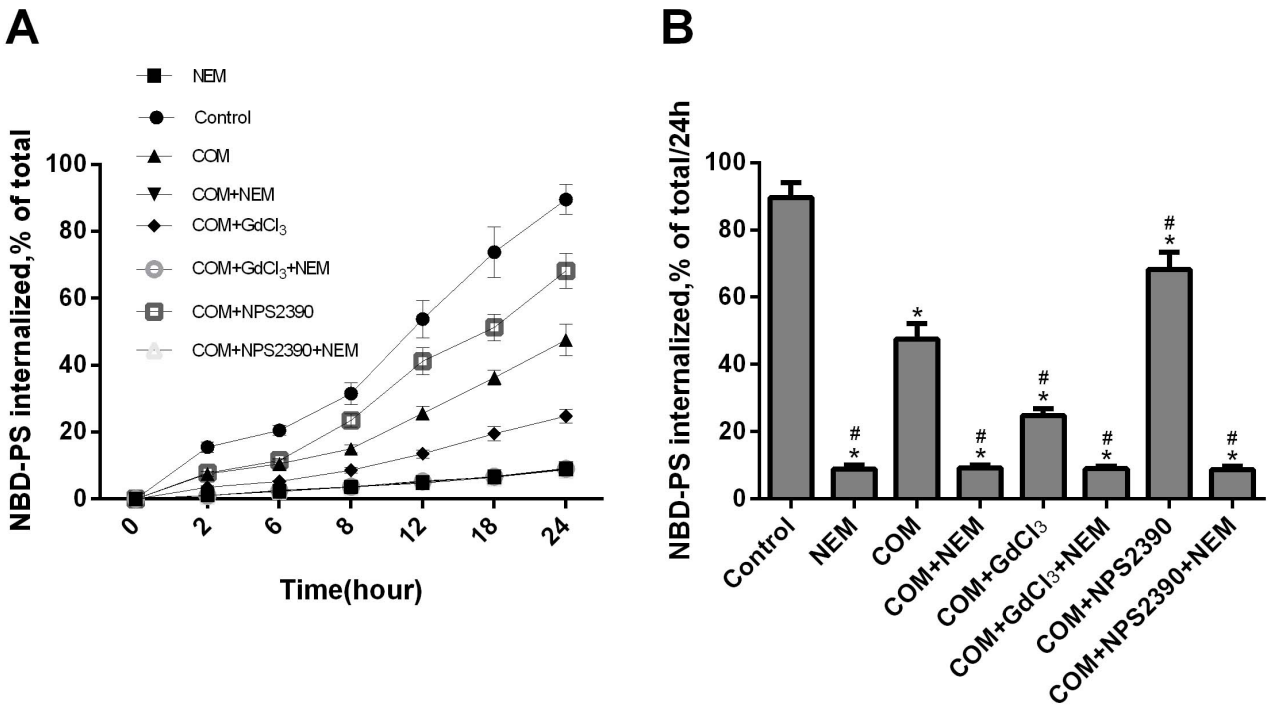

Fig. 4. NBD-PS internalization in human renal epithelial cells treated with COM in the presence or absence of NPS2390 or $GdCl_3$. NBD-PS was incorporated into the outer leaflet of the plasma membrane to assess inward PS transport. Cells were treated with COM crystals in the presence or absence of NPS2390 (10 μM, 1 h pretreatment) or $GdCl_3$ (300 μM, 30 min pretreatment). N-ethylmaleimide (NEM, 5 mM, 15 min) was used as an APLT inhibitor. (A) Time course of NBD-PS internalization. (B) Quantification of NBD-PS internalization at 24 h. Data are presented as mean ± SEM from three independent biological replicates. $^{*}p < 0.05$ versus Control without NEM; $^{\#}p < 0.05$ versus COM.

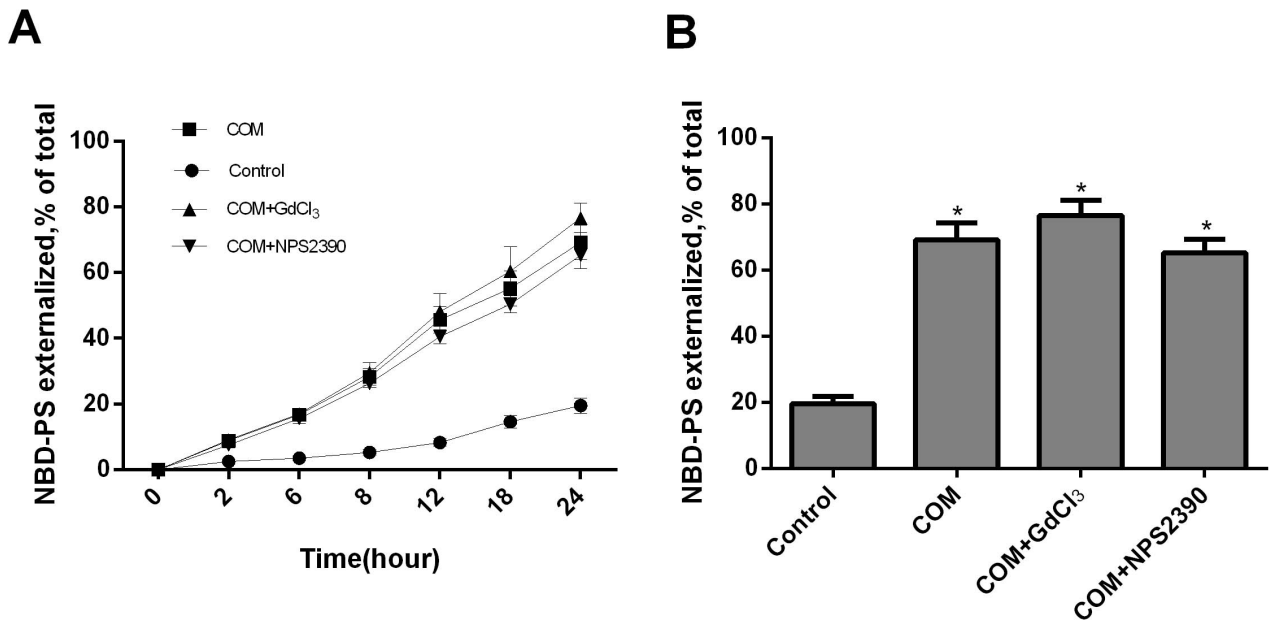

Fig. 5. NBD-PS externalization in human renal epithelial cells treated with COM in the presence or absence of NPS2390 or $GdCl_3$. NBD-PS was incorporated into the inner leaflet of the plasma membrane to assess outward PS redistribution. Cells were treated with COM crystals in the presence or absence of NPS2390 (10 μM, 1 h pretreatment) or $GdCl_3$ (300 μM, 30 min pretreatment). (A) Time course of NBD-PS externalization. (B) Quantification of NBD-PS externalization at 24 h. Data are presented as mean ± SEM from three independent biological replicates. $^{*}p < 0.05$ versus Control.

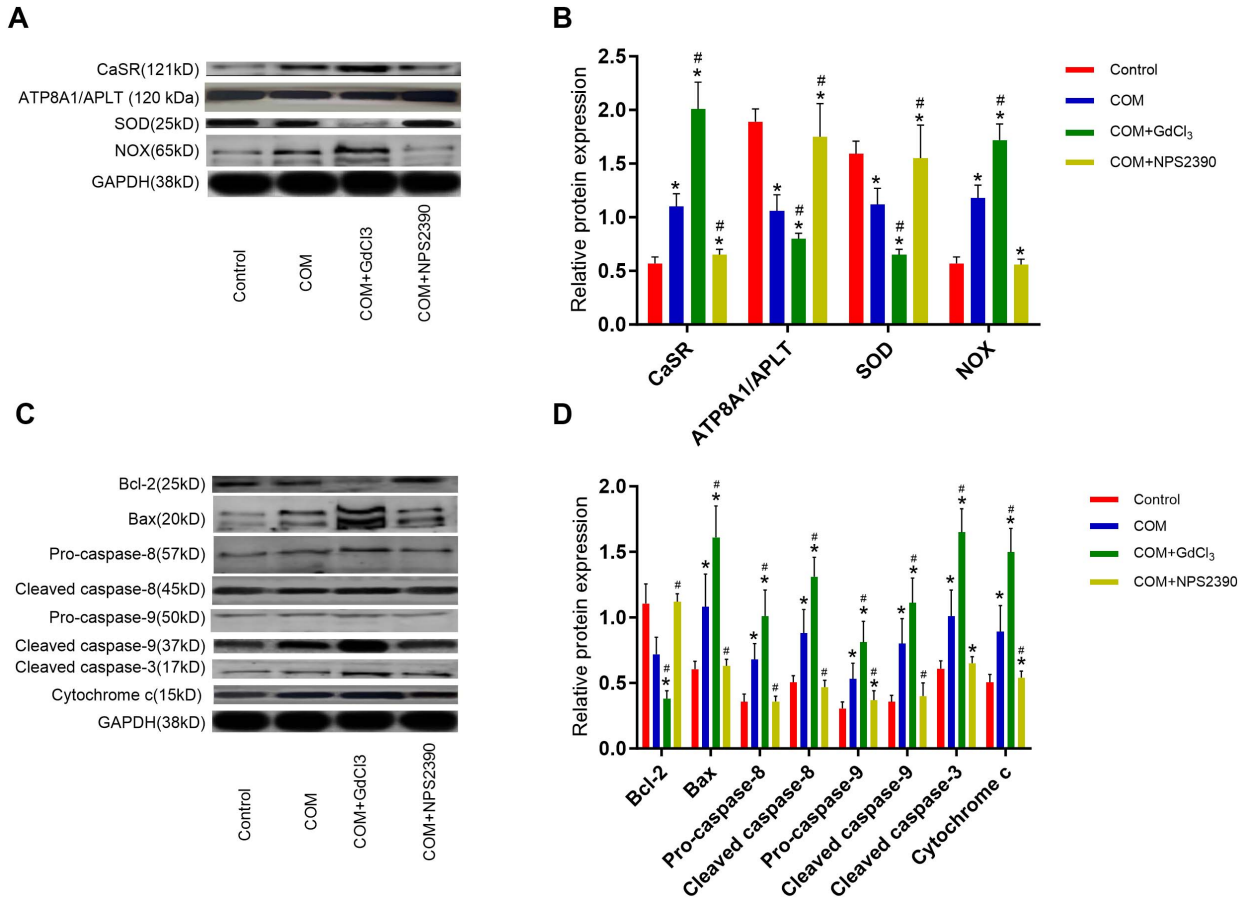

Fig. 6. Effects of COM and CaSR modulation on ATP8A1/APLT, oxidative-stress-related proteins, and apoptosis-related proteins in HK-2 cells. Cells were treated with COM crystals in the presence or absence of $GdCl_3$ or NPS2390. (A) Representative western blot images showing CaSR, ATP8A1/APLT, SOD, and NOX in the Control, COM, COM+$GdCl_3$, and COM+NPS2390 groups. (B) Densitometric quantification of CaSR, ATP8A1/APLT, SOD, and NOX. (C) Representative western blot images showing Bcl-2, Bax, pro-caspase-8, cleaved caspase-8, pro-caspase-9, cleaved caspase-9, cleaved caspase-3, and cytochrome c. (D) Densitometric quantification of apoptosis-related proteins. GAPDH was used as the loading control. Densitometric values for each target protein were normalized to the corresponding GAPDH signal and are presented as relative protein expression. Data are presented as mean ± SEM from three independent biological replicates. $^{*}p < 0.05$ versus Control; $^{\#}p < 0.05$ versus COM. COM, calcium oxalate monohydrate; CaSR, calcium-sensing receptor; APLT, aminophospholipid translocase; SOD, superoxide dismutase; NOX, NADPH oxidase.

and thereby minimizes interference from APLT-mediated inward transport. In control cells, approximately 20% of NBD-PS was transported to the outer leaflet within 24 h (Fig. 5B), possibly reflecting basal floppase activity. COM crystal treatment (67 μg/cm^2) increased outward NBD-PS transport to approximately 70% at 24 h ($p < 0.05$). However, neither $GdCl_3$ nor NPS2390 significantly altered this COM-induced outward redistribution, suggesting that COM-induced outward PS transport is largely CaSR-insensitive under our experimental conditions (Fig. 5B).

Taken together, COM was associated with a CaSR-sensitive defect in APLT-dependent inward PS flipping (NEM-sensitive), whereas COM-enhanced outward PS redistribution appeared CaSR-insensitive under our experimental conditions. This CaSR-insensitive outward redistribution may involve CaSR-independent scramblase pathways, such as Ca^{2+}-activated TMEM16F/ANO6 or apoptosis-associated XK-related (XKR) family proteins [23,24,25]. Because these candidates were not directly examined in the present study, their potential involvement remains to be validated.

3.6 Western Blot Analysis

CaSR was detected in all groups and was upregulated after COM treatment (Fig. 6A). CaSR levels in the COM + $GdCl_3$ group were greater than those in the COM group ($p < 0.05$) (Fig. 6B). Conversely, CaSR levels were lower in the COM + NPS2390 group than in the COM group ($p < 0.05$) (Fig. 6B). After COM treatment, APLT and SOD expression were downregulated, and nicotinamide adenine dinucleotide phosphate oxidase (NOX) levels were upregulated ($p < 0.05$).

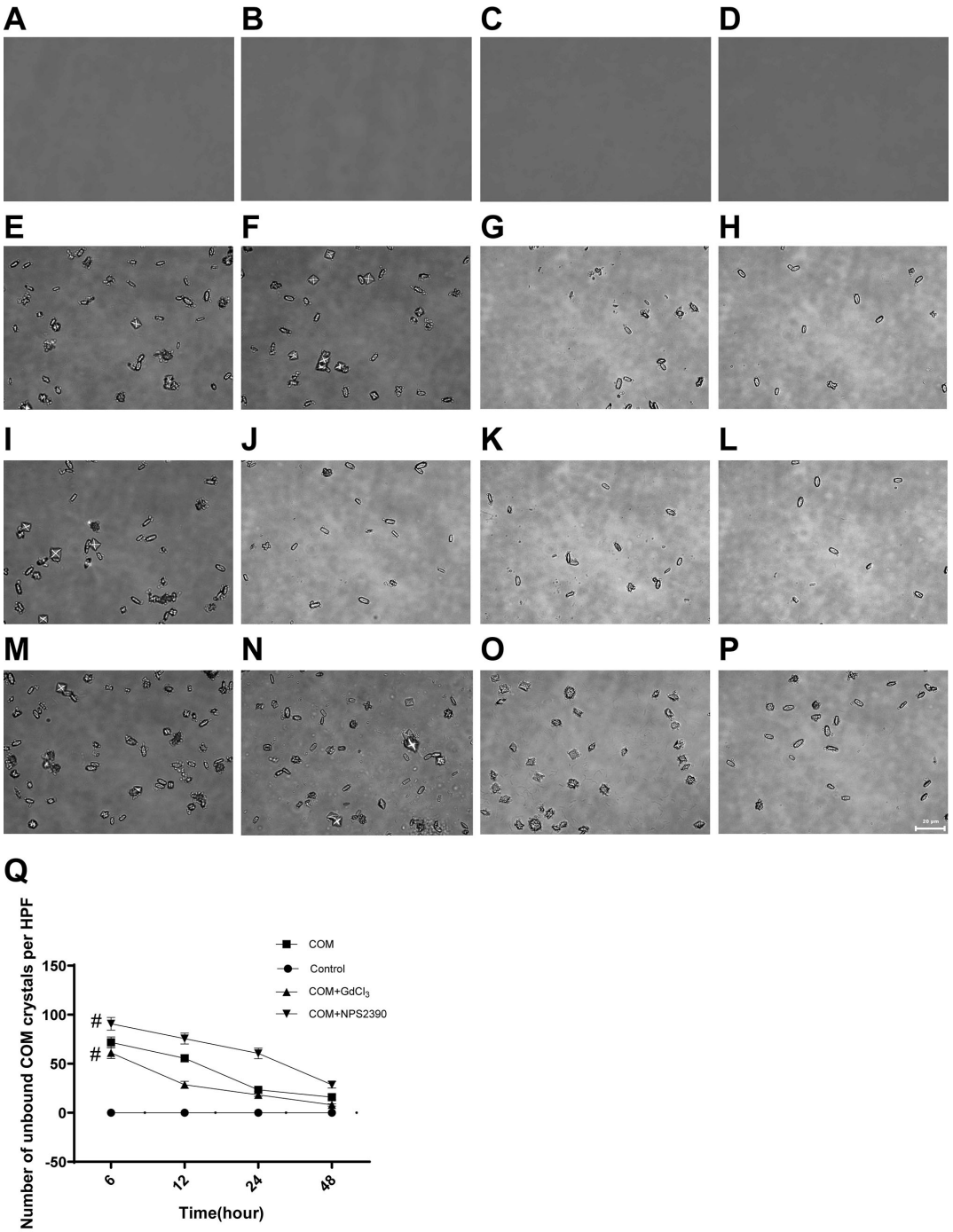

Fig. 7. COM crystal adhesion assay. Cells were treated with COM crystals for 6, 12, 24, or 48 h, and unbound crystals were collected and counted under phase-contrast microscopy. Representative images are shown for the Control group at 6, 12, 24, and 48 h (A–D); COM group (E–H); COM+$GdCl_3$ group (I–L); and COM+NPS2390 group (M–P). (Q) Quantification of unbound COM crystals per high-power field. Fewer unbound crystals indicate greater COM crystal adhesion/retention on the cell monolayer. Data are presented as mean ± SEM from three independent biological replicates. $^{\#}p < 0.05$ versus COM. Scale bar = 20 µm for panels A–P.

Upregulation of APLT and SOD expression and downregulation of NOX expression were observed in the COM + NPS2390 group compared to the COM group ($p < 0.05$). APLT and SOD expression were lower in the COM + $GdCl_3$ group than in the COM group. NOX expression, in contrast, was higher ($p < 0.05$) (Fig. 6B).

COM enhanced the levels of cytochrome c, cleaved caspase-3, cleaved caspase-8, cleaved caspase-9, pro-caspase-8, pro-caspase-9, and Bax and decreased Bcl-2 levels ($p < 0.05$; Fig. 6C,D). Compared with the COM group, this effect was reversed by NPS2390 but enhanced by $GdCl_3$. Therefore, COM is associated with activation of

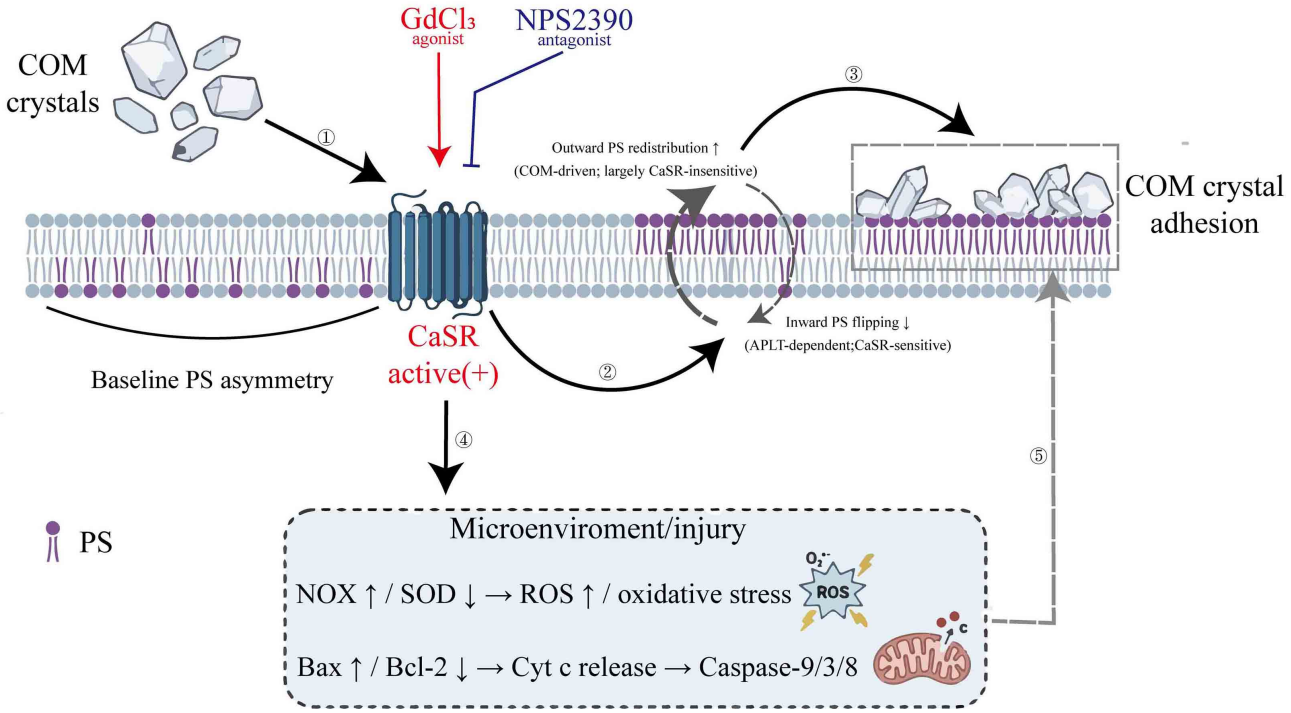

Fig. 8. Roles of the CaSR protein in stone formation. (1) Supersaturation of stone-forming components leads to COM crystal formation in the renal tubule lumen. Crystal–cell contact activates CaSR (enhanced by $GdCl_3$ and attenuated by NPS2390). (2) Under baseline conditions, PS is predominantly localized in the inner leaflet of the plasma membrane. CaSR activation may impair APLT-dependent inward PS transport. Together with COM-driven outward PS redistribution, PS becomes externalized on the epithelial surface and forms an anionic platform. (3) Surface PS exposure may provide a permissive anionic platform for COM crystal adhesion/retention. (4) COM exposure also elicits CaSR-sensitive oxidative stress and apoptosis-related signaling, including increased NOX expression, decreased SOD expression, and subsequent ROS accumulation. This pathway further triggers Bax upregulation, Bcl-2 downregulation, cytochrome c release, and activation of caspase-9/3 and caspase-8. (5) Sustained oxidative imbalance and epithelial injury may create a retention-favorable epithelial state. The dashed arrow indicates an interpretive link based on the present findings rather than a direct causal pathway.

the caspase cascade in a CaSR-sensitive manner, which is consistent with apoptosis-related signaling in human renal epithelial cells.

3.7 Crystal Adherence to Cells in Groups

Compared with COM alone, $GdCl_3$ significantly decreased the number of unbound crystals, indicating increased crystal adhesion/retention on the cell monolayer (Fig. 7) ($p < 0.05$). In contrast, NPS2390 increased the number of unbound crystals, indicating reduced crystal adhesion/retention compared with COM alone ($p < 0.05$). Crystal adherence to cells subjected to varying exposure durations (6, 12, 24, or 48 h) was also determined in the four groups. The response was time-dependent. Fig. 7 indicates that crystal adherence to human renal epithelial cells was the highest at the 48 h time point.

4. Discussion

COM plays an important role in CaOx stone formation and can impair tubular epithelial cell function [26]. However, the mechanisms by which renal tubular cells respond to COM remain incompletely understood. Therefore, we performed differential proteomic analysis to identify COM-induced protein alterations in renal tubular epithelial cells (Fig. 1 and Table 1). Quantitative 2-DE identified 11 differential spots (>1.5-fold), corresponding to 8 unique proteins. These proteins included factors implicated in redox/stress responses (e.g., PRDX1), membrane-associated processes (e.g., ANXA2), and structural organization (e.g., LMNA), providing a proteomic context for subsequent targeted experiments. Among the candidates, CaSR offered a receptor-level, pharmacologically addressable entry point for mechanistic testing.

Increasing evidence has revealed that CaSR may be involved in urolithiasis formation [27,28,29]. Our previous study revealed that activation of CaSR by COM may lead to crystallization adhesion and subsequent renal insufficiency [12]. In a rat model, CaSR activation was further associated with increased oxidative stress and PS externalization and could be modulated in the same pharmacologic direc-

tion [30]. These studies established CaSR as a relevant upstream signal in COM-related tubular injury and crystal retention. However, the mechanism linking CaSR activation to crystal adhesion remains unclear. Studies have shown that the appearance of extracellular PS in renal epithelial cells may promote the adhesion of COM crystals on the cell membrane [31]. Therefore, we hypothesized that CaSR activation may be associated with COM-induced disturbance of PS membrane asymmetry in renal epithelial cells.

In our study, we observed a COM-induced increase in CaSR expression together with elevated cell-surface PS exposure and enhanced crystal adhesion in human renal epithelial cells. Pharmacologic modulation of CaSR showed consistent directional effects: the CaSR inhibitor NPS2390 attenuated, whereas the CaSR activator $GdCl_3$ augmented, COM-associated PS exposure and crystal adhesion, with parallel changes in oxidative stress and apoptosis-related readouts. However, these parallel changes should be interpreted as associative rather than definitive causal evidence that PS exposure directly mediates crystal adhesion.

In addition, COM markedly enhanced the outward movement of NBD-PS; however, altering CaSR activity did not significantly change this outward redistribution, suggesting that COM-enhanced outward PS movement is largely CaSR-insensitive under our experimental conditions (Fig. 5). In contrast, COM impaired the inward movement of NBD-PS, and this defect was alleviated by NPS2390 but further aggravated by $GdCl_3$, suggesting a CaSR-sensitive impairment of APLT-dependent inward PS transport (inward flipping). To our knowledge, the relative contribution of outward redistribution versus impaired inward flipping to COM-induced surface PS exposure has been less well characterized in the context of CaSR modulation [9]. Thus, impaired inward flipping may contribute to net surface PS enrichment, thereby providing a permissive anionic platform that may favor COM crystal–cell interactions [31]. This interpretation is further supported by the CaSR-sensitive changes in APLT expression and by the directional effects of $GdCl_3$ and NPS2390 on inward NBD-PS transport.

Renal tubular epithelial injury and cell death may promote crystallization by generating cellular debris and membrane-derived vesicles that can facilitate heterogeneous nucleation and enhance crystal–cell interactions [32,33]. Because epithelial injury and cell death may facilitate crystal retention, we further evaluated apoptosis-related signaling in COM-treated HK-2 cells. Apoptosis is regulated by a balance between pro- and anti-apoptotic proteins, including Bax and Bcl-2, and by downstream caspase activation [34]. Based on our Western blot results, we assessed apoptosis-related signaling by examining caspase-3, caspase-9 and caspase-8. We observed that COM increased cytochrome c release and the cleavage/activation of caspase-3/8/9 together with Bax upregulation and Bcl-2 downregulation, and these changes were sensitive to CaSR modulation (NPS2390 attenuated, whereas $GdCl_3$ enhanced them), suggesting that COM-triggered apoptosis-related signaling in HK-2 cells is CaSR-sensitive.

Studies have shown that oxalate-induced increases in ROS production decrease the activity of APLT, and reduced APLT activity plays an important role in CaOx calculus formation by promoting the redistribution of PS in renal epithelial cells [10]. Consistent with this concept, we observed COM-induced oxidative stress accompanied by reduced APLT expression, supporting a potential link between oxidative stress and impaired inward PS flipping in this model. Increased ROS may further promote crystal aggregation, nucleation, and growth, partly by aggravating epithelial injury and membrane-vesicle generation, thereby enhancing crystal retention and cell–crystal interactions [35,36,37]. Consistent with an injury-associated response, COM was associated with CaSR-sensitive changes in mitochondrial apoptosis-related proteins, including Bax/Bcl-2 imbalance, cytochrome c release, and cleavage/activation of caspase-9/3 and caspase-8, which were attenuated by NPS2390 and enhanced by $GdCl_3$. These CaSR-linked oxidative and apoptotic responses likely reflect epithelial stress accompanying COM exposure and may further create a microenvironment that favors crystal retention, while the proposed PS-related adhesion axis in our model is primarily supported by impaired APLT-dependent inward PS transport. In our study, pharmacologic modulation of CaSR consistently altered oxidative-stress-related markers (LDH, MDA, SOD, and NOX), apoptosis-related signaling, APLT expression, and PS exposure, in parallel with changes in crystal adhesion. Together, these data support a model in which COM is associated with CaSR-sensitive oxidative and apoptosis-related responses and impaired APLT-dependent inward PS transport, which may favor sustained surface PS exposure and create a permissive membrane environment for COM crystal–cell adhesion (Fig. 8), while outward PS redistribution was not significantly altered by CaSR modulation (Fig. 5) and thus appears largely CaSR-insensitive under our conditions, potentially involving CaSR-independent pathways.

Limitations

Although surface PS exposure is a plausible anionic platform for CaOx crystal binding as reported previously, we did not directly manipulate PS externalization (e.g., masking surface PS or selectively modulating scramblase/flippase activity) to establish causality between PS exposure and crystal adhesion in our system; therefore, it should be interpreted as a potential contributor rather than a definitive mediator of COM crystal–cell adhesion. In addition, Annexin V staining was performed without viability dyes such as propidium iodide (PI) or 7-aminoactinomycin D (7-AAD); therefore, increased Annexin V positivity should be interpreted as an index of surface PS exposure under COM-induced injury conditions,

rather than as direct evidence of selective PS redistribution in viable cells. Nevertheless, the concordant changes in PS exposure/PS translocation and crystal adhesion under CaSR modulation, together with the observed CaSR-sensitive defect in APLT-dependent inward flipping, support our proposed model that impaired membrane phospholipid asymmetry may favor crystal retention. Another limitation is that our mechanistic interpretation relies on pharmacologic modulation of CaSR using $GdCl_3$ and NPS2390. Although the opposite directional effects of these two agents support CaSR involvement, potential off-target effects cannot be fully excluded, and genetic validation using CaSR knockdown, knockout, or rescue approaches was not performed. In addition, apoptosis was inferred from apoptosis-related protein changes rather than direct functional assays such as terminal deoxynucleotidyl transferase-mediated dUTP nick-end labeling (TUNEL) staining, caspase activity measurements, or mitochondrial membrane potential analysis. Oxidative stress was assessed using LDH, MDA, SOD, and NOX-related measurements, which do not fully define the upstream oxidative signaling pathways involved. Finally, while outward PS redistribution appeared largely CaSR-insensitive in our assays, the upstream drivers of this outward process were not directly interrogated. Future studies using direct PS-targeting or gene-silencing approaches will be valuable to further test the causal contribution of PS externalization and CaSR signaling to crystal–cell adhesion.

5. Conclusions

Our findings show that COM exposure increased CaSR expression in renal tubular epithelial cells and was accompanied by oxidative stress, apoptosis-related signaling, and enhanced crystal adhesion. Mechanistically, COM induced a pharmacologically CaSR-sensitive defect in APLT-dependent inward PS transport (inward flipping), whereas COM-enhanced outward PS redistribution was largely CaSR-insensitive under our experimental conditions. This imbalance may favor sustained PS exposure on the cell surface, providing a potential anionic platform for COM crystal–cell adhesion. However, the direct causality between PS exposure and COM crystal–cell adhesion remains to be further validated. Pharmacologic inhibition of CaSR attenuated these abnormalities, supporting CaSR as a potential target to reduce COM-induced epithelial injury and crystal retention.

Abbreviations

APLT, aminophospholipid translocase; CaOx, calcium oxalate; CaSR, calcium-sensing receptor; COM, calcium oxalate monohydrate; LDH, lactate dehydrogenase; MDA, malondialdehyde; OS, oxidative stress; PS, phosphatidylserine; ROS, reactive oxygen species; SOD, superoxide dismutase.

Availability of Data and Materials

The datasets generated and analyzed during the current study are available from the corresponding authors on reasonable request.

Author Contributions

HL, YX contributed equally to this work. XL, HL and WS conceived and designed the study. YX performed the experiments and collected the data. YF and SC contributed to data curation, figure preparation, and statistical analyses. HL performed data analysis and interpretation. XL provided materials/reagents/analytical tools and technical support. HL drafted the manuscript. HL and WS critically revised the manuscript for important intellectual content. WS and XL supervised the study and coordinated the project. All authors contributed to critical revision of the manuscript for important intellectual content. All authors read and approved the final manuscript. All authors have participated sufficiently in the work and agreed to be accountable for all aspects of the work.

Ethics Approval and Consent to Participate

Not applicable. This study did not involve human participants or animals.

Acknowledgment

Not applicable.

Funding

This research received no external funding.

Conflicts of Interest

The authors declare no conflicts of interest.

Supplementary Material

Supplementary material associated with this article can be found, in the online version, at https://doi.org/10.31083/FBL53201.

References

[1] Bamberger JN, Blum KA, Kan KM, Parkhomenko E, Gallante B, Gupta M. Clinical and Metabolic Correlates of Calcium Oxalate Stone Subtypes: Implications for Etiology and Management. Journal of Endourology. 2019; 33: 755–760. https://doi.org/10.1089/end.2019.0245

[2] Zhao Y, Yang B, Yang X, Zhou H, Zhao H, Yue R, et al. Exploring the Interplay between Calcium Oxalate Crystals and Renal Tubular Epithelial Cell Injury: Implications for the Formation and Prevention of Kidney Stones. Integrative Medicine in Nephrology and Andrology. 2024; 11: e23-00022. https://doi.org/10.1097/IMNA-D-23-00022

[3] Wang B, He G, Xu G, Wen J, Yu X. miRNA-34a inhibits cell adhesion by targeting CD44 in human renal epithelial cells: implications for renal stone disease. Urolithiasis. 2020; 48: 109–116. https://doi.org/10.1007/s00240-019-01155-9

[4] Lieske JC, Norris R, Swift H, Toback FG. Adhesion, internalization and metabolism of calcium oxalate monohydrate crystals by renal epithelial cells. Kidney International. 1997; 52: 1291–1301. https://doi.org/10.1038/ki.1997.454
[5] Manissorn J, Fong-Ngern K, Peerapen P, Thongboonkerd V. Systematic evaluation for effects of urine pH on calcium oxalate crystallization, crystal-cell adhesion and internalization into renal tubular cells. Scientific Reports. 2017; 7: 1798. https://doi.org/10.1038/s41598-017-01953-4
[6] Cao LC, Jonassen J, Honeyman TW, Scheid C. Oxalate-induced redistribution of phosphatidylserine in renal epithelial cells: implications for kidney stone disease. American Journal of Nephrology. 2001; 21: 69–77. https://doi.org/10.1159/000046224
[7] Wiessner JH, Hasegawa AT, Hung LY, Mandel NS. Oxalate-induced exposure of phosphatidylserine on the surface of renal epithelial cells in culture. Journal of the American Society of Nephrology : JASN. 1999; 10: S441–S445.
[8] Schroit AJ, Zwaal RF. Transbilayer movement of phospholipids in red cell and platelet membranes. Biochimica et Biophysica Acta. 1991; 1071: 313–329. https://doi.org/10.1016/0304-4157(91)90019-s
[9] Nagata S, Sakuragi T, Segawa K. Flippase and scramblase for phosphatidylserine exposure. Current Opinion in Immunology. 2020; 62: 31–38. https://doi.org/10.1016/j.coi.2019.11.009
[10] Yu SL, Gan XG, Huang JM, Cao Y, Wang YQ, Pan SH, et al. Oxalate impairs aminophospholipid translocase activity in renal epithelial cells via oxidative stress: implications for calcium oxalate urolithiasis. The Journal of Urology. 2011; 186: 1114–1120. https://doi.org/10.1016/j.juro.2011.04.106
[11] Devaux PF, López-Montero I, Bryde S. Proteins involved in lipid translocation in eukaryotic cells. Chemistry and Physics of Lipids. 2006; 141: 119–132. https://doi.org/10.1016/j.chemphyslip.2006.02.007
[12] Li X, Ma J, Shi W, Su Y, Fu X, Yang Y, et al. Calcium Oxalate Induces Renal Injury through Calcium-Sensing Receptor. Oxidative Medicine and Cellular Longevity. 2016; 2016: 5203801. https://doi.org/10.1155/2016/5203801
[13] Segawa K, Nagata S. An Apoptotic 'Eat Me' Signal: Phosphatidylserine Exposure. Trends in Cell Biology. 2015; 25: 639–650. https://doi.org/10.1016/j.tcb.2015.08.003
[14] Shlomovitz I, Speir M, Gerlic M. Flipping the dogma - phosphatidylserine in non-apoptotic cell death. Cell Communication and Signaling : CCS. 2019; 17: 139. https://doi.org/10.1186/s12964-019-0437-0
[15] Khan SR, Khan A, Byer KJ. Temporal changes in the expression of mRNA of NADPH oxidase subunits in renal epithelial cells exposed to oxalate or calcium oxalate crystals. Nephrology, Dialysis, Transplantation : Official Publication of the European Dialysis and Transplant Association - European Renal Association. 2011; 26: 1778–1785. https://doi.org/10.1093/ndt/gfq692
[16] Zuo J, Khan A, Glenton PA, Khan SR. Effect of NADPH oxidase inhibition on the expression of kidney injury molecule and calcium oxalate crystal deposition in hydroxy-L-proline-induced hyperoxaluria in the male Sprague-Dawley rats. Nephrology, Dialysis, Transplantation : Official Publication of the European Dialysis and Transplant Association - European Renal Association. 2011; 26: 1785–1796. https://doi.org/10.1093/ndt/gfr035
[17] Byer K, Khan SR. Citrate provides protection against oxalate and calcium oxalate crystal induced oxidative damage to renal epithelium. The Journal of Urology. 2005; 173: 640–646. https://doi.org/10.1097/01.ju.0000143190.49888.c7
[18] Thamilselvan S, Byer KJ, Hackett RL, Khan SR. Free radical scavengers, catalase and superoxide dismutase provide protection from oxalate-associated injury to LLC-PK1 and MDCK cells. The Journal of Urology. 2000; 164: 224–229.
[19] Jones-Isaac K, Yeung CK, Bain J, Lidberg K, Yang J, Wang L, et al. Effect of calcium oxalate microcrystals on kidney proximal tubule epithelial cell gene expression in microgravity. NPJ Microgravity. 2025; 12: 2. https://doi.org/10.1038/s41526-025-00543-3
[20] McIntyre JC, Sleight RG. Fluorescence assay for phospholipid membrane asymmetry. Biochemistry. 1991; 30: 11819–11827. https://doi.org/10.1021/bi00115a012
[21] Pohl A, Lage H, Müller P, Pomorski T, Herrmann A. Transport of phosphatidylserine via MDR1 (multidrug resistance 1)P-glycoprotein in a human gastric carcinoma cell line. The Biochemical Journal. 2002; 365: 259–268. https://doi.org/10.1042/BJ20011880
[22] Kanlaya R, Fong-Ngern K, Thongboonkerd V. Cellular adaptive response of distal renal tubular cells to high-oxalate environment highlights surface alpha-enolase as the enhancer of calcium oxalate monohydrate crystal adhesion. Journal of proteomics. 2013; 80: 55–65. https://doi.org/10.1016/j.jprot.2013.01.001
[23] Suzuki J, Denning DP, Imanishi E, Horvitz HR, Nagata S. Xk-related protein 8 and CED-8 promote phosphatidylserine exposure in apoptotic cells. Science (New York, N.Y.). 2013; 341: 403–406. https://doi.org/10.1126/science.1236758
[24] Suzuki J, Imanishi E, Nagata S. Xkr8 phospholipid scrambling complex in apoptotic phosphatidylserine exposure. Proceedings of the National Academy of Sciences of the United States of America. 2016; 113: 9509–9514. https://doi.org/10.1073/pnas.1610403113
[25] Yu K, Whitlock JM, Lee K, Ortlund EA, Cui YY, Hartzell HC. Identification of a lipid scrambling domain in ANO6/TMEM16F. elife. 2015; 4: e06901. https://doi.org/10.7554/eLife.06901
[26] Peerapen P, Thongboonkerd V. Effects of calcium oxalate monohydrate crystals on expression and function of tight junction of renal tubular epithelial cells. Laboratory Investigation; a Journal of Technical Methods and Pathology. 2011; 91: 97–105. https://doi.org/10.1038/labinvest.2010.167
[27] Vezzoli G, Scillitani A, Corbetta S, Terranegra A, Dogliotti E, Guarnieri V, et al. Risk of nephrolithiasis in primary hyperparathyroidism is associated with two polymorphisms of the calcium-sensing receptor gene. Journal of Nephrology. 2015; 28: 67–72. https://doi.org/10.1007/s40620-014-0106-8
[28] Walker RW, Zhang S, Coleman-Barnett JA, Hamm LL, Hering-Smith KS. Calcium receptor signaling and citrate transport. Urolithiasis. 2018; 46: 409–418. https://doi.org/10.1007/s00240-018-1035-0
[29] Luo P, Chen T, Zheng L, Zou J, Zou J, Li W, et al. Calcium sensing receptor regulate claudin-14 via PKA-STAT3 pathway in rat model of nephrolithiasis. Frontiers in Pharmacology. 2024; 15: 1477122. https://doi.org/10.3389/fphar.2024.1477122
[30] Li X, Chen S, Feng D, Fu Y, Wu H, Lu J, et al. Calcium-sensing receptor promotes calcium oxalate crystal adhesion and renal injury in Wistar rats by promoting ROS production and subsequent regulation of PS ectropion, OPN, KIM-1, and ERK expression. Renal Failure. 2021; 43: 465–476. https://doi.org/10.1080/0886022X.2021.1881554
[31] Bigelow MW, Wiessner JH, Kleinman JG, Mandel NS. Surface exposure of phosphatidylserine increases calcium oxalate crystal attachment to IMCD cells. The American Journal of Physiology. 1997; 272: F55–F62. https://doi.org/10.1152/ajprenal.1997.272.1.F55
[32] Fasano JM, Khan SR. Intratubular crystallization of calcium oxalate in the presence of membrane vesicles: an in vitro study. Kidney International. 2001; 59: 169–178. https://doi.org/10.1046/j.1523-1755.2001.00477.x
[33] Tsujihata M. Mechanism of calcium oxalate renal stone formation and renal tubular cell injury. International Journal of Urol-

ogy : Official Journal of the Japanese Urological Association. 2008; 15: 115–120. https://doi.org/10.1111/j.1442-2042.2007.01953.x

[34] Shen Y, Huang G, Liu Y, Pan F, Long C, Liu J, Ma Z. P110 Inhibits DRP1/FIS1-Mediated Mitochondrial Fission to Alleviate Uric Acid-Induced Apoptosis in HK-2 Cells. Frontiers in Bioscience (Landmark Edition). 2025; 30: 46700. https://doi.org/10.31083/FBL46700

[35] Sun Y, Sun H, Zhang Z, Tan F, Qu Y, Lei X, et al. New insight into oxidative stress and inflammatory responses to kidney stones: Potential therapeutic strategies with natural active ingredients. Biomedicine & Pharmacotherapy = Biomedecine & Pharmacotherapie. 2024; 179: 117333. https://doi.org/10.1016/j.biopha.2024.117333

[36] Boldt AM, Di Sole F. Targeting the NLRP3 inflammasome for calcium oxalate stones: pathophysiology and emerging pharmacological interventions. Frontiers in Physiology. 2025; 16: 1614438. https://doi.org/10.3389/fphys.2025.1614438

[37] Lertprapai C, Peerapen P, Thongboonkerd V. Effects of calcium oxalate crystals on neutrophil cellular proteome and functions: implications for nephrolithiasis. Cell Communication and Signaling : CCS. 2025; 23: 336. https://doi.org/10.1186/s12964-025-02345-2